Investigation of Sm2+ as a near-infrared emitting activator for NaI scintillators

van Aarle, Casper; Biner, Daniel A.; Krämer, Karl W.; Dorenbos, Pieter

DOI
10.1016/j.optmat.2024.116094

Publication date
2024

Document Version
Final published version

Published in
Optical Materials

Optical Materials 157 (2024) 116094

Contents lists available at ScienceDirect

Optical Materials

journal homepage: www.elsevier.com/locate/optmat

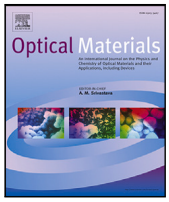

Research article

Investigation of Sm^{2+} as a near-infrared emitting activator for NaI scintillators

Casper van Aarle [a,*], Daniel A. Biner [b], Karl W. Krämer [b], Pieter Dorenbos [a]

[a] Faculty of Applied Sciences, Delft University of Technology, Mekelweg 15, Delft, The Netherlands
[b] Department of Chemistry and Biochemistry, University of Bern, Freiestrasse 3, Bern, Switzerland

ARTICLE INFO

Keywords:
Scintillator
Samarium
NaI
Single crystal
Near-infrared emission

ABSTRACT

NaI is the most commonly used host lattice for scintillators, which makes it interesting to further improve its scintillation properties. Many alternative activators have been tried instead of the conventionally used Tl^+. In this work, Sm^{2+} is used as an near-infrared emitting activator for NaI to study whether it is suitable for readout with silicon based photodetectors. NaI single crystals (co-)doped with 0-0.2% Tl^+ and 0.2%–2% Sm^{2+} were grown by the vertical Bridgman technique. The emission of the samples was studied under optical and X-ray excitation. It is shown by photoluminescence decay studies that Tl^+ works as a sensitiser for Sm^{2+}. The samples indicate the formation of multiple (at least 5) different Sm^{2+} emission sites. Annealing the samples changes their emission intensity and scintillation properties. NaI:Sm^{2+} shows great similarities with its Eu^{2+}-doped counterpart. Finally, it is demonstrated that NaI:Sm^{2+} can be read out with silicon photomultipliers and an energy resolution of 11% has been attained.

1. Introduction

NaI:Tl^+ has been in use since the earliest times of scintillation research and was used in the first scintillation counter developed by Hofstadter [1–3]. Ever since, scintillation detectors containing NaI:Tl^+ have become widely available commercial products. Scintillation detectors with a NaI:Tl^+ crystal typically reach an energy resolution of around 6% at 662 keV [4].

Later research on scintillation materials has shown that the energy resolution is strongly related to proportionality of the scintillator's response to different γ-ray energies [5]. A more proportional response leads to a better energy resolution. It was shown by Moszynski et al. that the proportionality of NaI considerably worsens due to Tl^+-doping [6–8]. They demonstrated that with undoped NaI, which scintillates at 78 K, an energy resolution of 3.7% can be attained [9].

The knowledge that dopants can influence the energy resolution of a scintillation detector has sparked research into improving scintillators through co-doping. This co-doping was primarily done with ions that are optically inactive, so that its spectroscopic properties are minimally affected. This research has for example led to an improvement of the energy resolution of $LaBr_3$:Ce^{3+} scintillation detectors. Co-doping with a few ppm of Sr^{2+} resulted in an energy resolution of 2.04% [10], compared to the 2.8% attained without co-doping [11]. A similar co-doping strategy has been applied to improve the energy resolution of NaI:Tl^+. Several studies report minor improvements in energy resolution upon co-doping with alkaline earth ions [12–14]. Besides, the (co-)doping of NaI with Eu^{2+} has also been studied [15–21].

As opposed to the alkaline earth metals, Eu^{2+} is optically active and shows $4f^65d \rightarrow 4f^7$ emission when doped in NaI. Fig. 2a shows the emission spectrum of NaI:Eu at room temperature as measured by Shiran et al. [17]. The emission spectrum contains several overlapping bands with maxima ranging from 410 nm to 490 nm. The configurational coordinate diagram in Fig. 2b shows the $4f^7$ ground state and $4f^65d$ excited state on Eu^{2+} for an emission wavelength of 440 nm (the emission maximum in Fig. 2a) and a typical Stokes shift of 0.25 eV [23]. The diagram shows that the $4f^65d \rightarrow 4f^7$ transition of Eu^{2+} only has one final state, meaning only one emission band can originate from a single site. For this reason the multiple emission bands in Fig. 2a have each been ascribed to different Eu^{2+} sites [16,17]. The prevalence of these sites is strongly dependent on Eu^{2+} concentration and thermal treatment of the crystal. When increasing the Eu^{2+} concentration from 0.15% to 0.25%, the intensity maximum of the emission spectrum shifts from 440 nm to 470 nm [17]. Additionally, the emission spectrum of NaI:Eu^{2+} crystals was found to slowly change over the course of months after synthesis.

While there appears to be no real consensus on the nature of the different Eu^{2+} sites in literature on NaI:Eu^{2+}, a vast amount of literature exists on the topic of divalent impurities in alkali halides. Doping alkali

* Corresponding author.
E-mail address: c.vanaarle@tudelft.nl (C. van Aarle).

https://doi.org/10.1016/j.optmat.2024.116094
Received 25 July 2024; Received in revised form 27 August 2024; Accepted 9 September 2024
Available online 12 September 2024

Fig. 1. Millimeter sized crystals of NaI:0.2%Sm^{2+} (left) and NaI:0.2%Tl^{+},0.2%Sm^{2+} (right) crystals sealed in silica ampoules.

halides with divalent impurities creates cation vacancies as charge compensation. These cation vacancies significantly increase the ionic conductivity, also at room temperature [24]. Meanwhile, the solubility of divalent impurities in alkali halides is low and strongly decreases with decreasing temperature [25]. This causes precipitation of the divalent impurities below a specific temperature, which lies at several 100 °C. As a result, crystals grown from a melt are often opaque [26]. Crystals can be made transparent again by annealing above the precipitation temperature and subsequently quenching the samples to room temperature. Such heat treatment is also mostly applied to NaI:Eu^{2+} crystals reported in literature [16,17,21].

The excitation bands of all observed Eu^{2+} sites overlap with the emission of Tl^{+} in NaI. This means that co-doping NaI:Tl^{+} with Eu^{2+} results in energy transfer from Tl^{+} to Eu^{2+} [18]. The efficiency depends primarily on the Eu^{2+} concentration. It was however concluded by Gridin et al. that the low solubility of Eu^{2+} makes it difficult to achieve efficient energy transfer from Tl^{+} to Eu^{2+} [19].

In recent years, silicon photomultipliers (SiPM) have been more commonly used as an alternative photodetector to a photomultiplier tube (PMT) [27–30]. While the best energy resolutions to date are still attained with PMTs, SiPMs offer several benefits. They are smaller than a PMT, not sensitive to magnetic fields and can be mass produced at low cost [31,32]. These benefits are particularly valuable when the energy resolution is primarily limited by the scintillator material, such as often the case with NaI. In this case, a small increase in detector noise or decrease in the detection efficiency of scintillation photons has a minor effect on the energy resolution. When the low cost and compactness of the scintillation detector are the most important criteria, SiPMs may be preferred over a PMT. While the detection efficiency of a PMT is highest in the UV or blue part of the electromagnetic spectrum, SiPMs can efficiently detect wavelengths up to 800 nm [33], which lies in the near-infrared (NIR). This makes Sm^{2+}, which emits in the NIR, an interesting alternative dopant to Eu^{2+}.

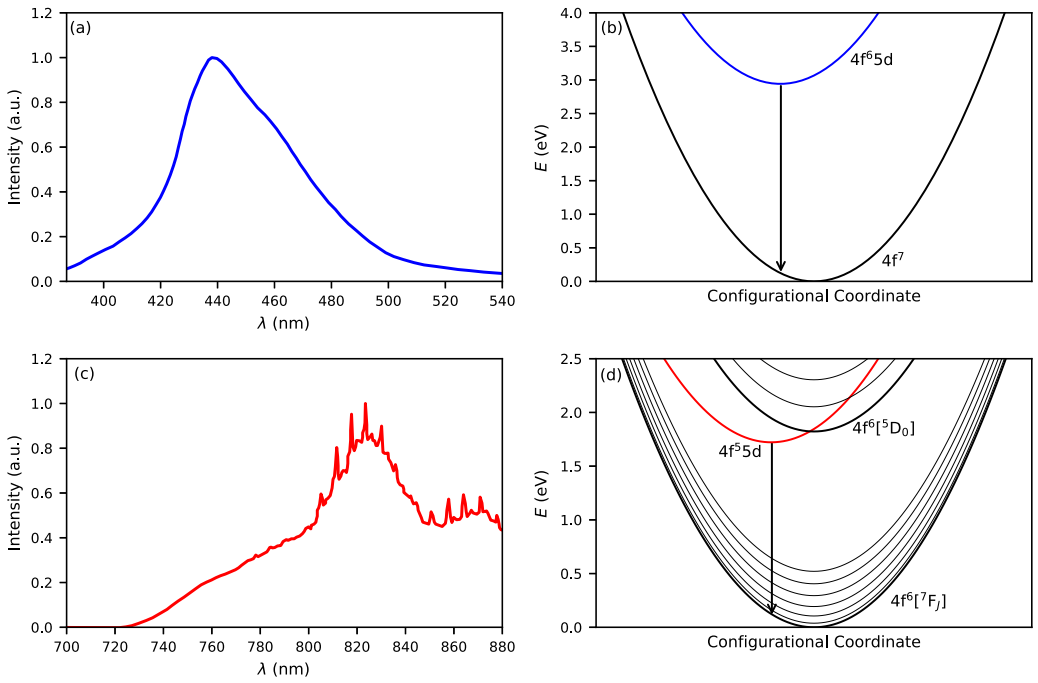

Fig. 2. (a) Photoluminescence emission spectrum of NaI:Eu^{2+} at room temperature taken from [17], (b) configurational coordinate diagram of Eu^{2+} for 440 nm emission wavelength and 0.25 eV Stokes shift, (c) photoluminescence emission spectrum of NaI:Sm^{2+} at 15 K taken from [22], (d) configurational coordinate diagram of Sm^{2+} assuming the same site as Eu^{2+} in (b).

The 15 K photoluminescence emission spectrum of NaI:0.3%Sm^{2+} single crystals was reported by Guzzi and Baldini [22], the spectrum is shown in Fig. 2c. Similar to the observations in NaI:Eu^{2+} (Fig. 2a), it shows multiple emission bands, this time between 750 nm and 880 nm. The spectrum is cut off at 880 nm due to the low sensitivity of the detector they used at longer wavelengths. The configurational coordinate diagram in Fig. 2d shows the configurational coordinate diagram assuming Sm^{2+} sits on the same site as Eu^{2+} in Fig. 2b. Sm^{2+} has the $4f^6[^7F_0]$ ground state configuration, which is part of the $4f^6[^7F_J]$ multiplet. Approximately 1.8 eV above the ground state lies the $4f^6[^5D_0]$ excited state [34], from which $4f^6 \rightarrow 4f^6$ line emission is observed in many different compounds [35–37]. Sm^{2+} also has many excited states belonging to the $4f^55d$ configuration, of which the state with lowest energy is drawn. When located on the same site as Eu^{2+}, the Sm^{2+} $4f^55d \rightarrow 4f^6[^7F_0]$ transition lies at 1.22 eV lower energy than the Eu^{2+} $4f^65d \rightarrow 4f^7$ transition, and the Stokes shift is the same [38]. Fig. 2d shows that the lowest $4f^55d$ excited state lies at lower energy than the $4f^6[^5D_0]$ state. Because of this, Sm^{2+} is expected to show broad band $4f^55d \rightarrow 4f^6$ emission, in accordance with the broad band emission shown in Fig. 2c. As transitions between the $4f^6$ and $4f^55d$ states are allowed, the decay time of the broad band $4f^55d \rightarrow 4f^6$ emission is typically around 2 μs [39]. Guzzi and Baldini reported a decay time shorter then 3 μs [22], which is fast enough for scintillator applications.

Sm^{2+} has several benefits compared to Eu^{2+}. Its $4f^6 \rightarrow 4f^55d$ transitions have a high absorption strength and their bands span across the entire optical spectrum, making Sm^{2+} easily sensitised by many other lanthanides [40–43], and other dopants such as Tl^+. Another benefit is that the $4f^55d \rightarrow 4f^6$ transition can have any of the $4f^6[^7F_J]$ states as final state. As absorption only takes place from the $4f^6[^7F_0]$ state, the probability of self-absorption in Sm^{2+}-doped scintillators is much lower than in their Eu^{2+}-doped counterparts, where the $4f^65d \rightarrow 4f^7$ transition only has a singular state as final state.

The shortest wavelength emission band in Fig. 2c has maximum intensity around 760 nm, while the longest reported emission band has a maximum around 870 nm. This emission band at 760 nm would be suitable for detection with silicon based photodetectors, while the wavelength of the emission band at 870 nm is too long for efficient detection. Knowledge on how the emission spectrum can be influenced is therefore necessary to make NaI:Sm^{2+} suitable for silicon based photodetector readout. For this reason, this work reports on the Sm^{2+} emission spectrum and compares it to its Eu^{2+} analogue, for which more spectroscopic information is available. The use of Tl^+ as a sensitiser for Sm^{2+} is assessed through photoluminescence excitation, emission, and decay measurements. Lastly, the effects of annealing and aging of NaI:Sm^{2+} on its scintillation properties are discussed.

2. Experimental techniques

Green, transparent crystals of NaI:2%Sm^{2+}, NaI:0.2%Sm^{2+}, and NaI:0.2%Tl^+,0.2%Sm^{2+} were grown from stoichiometric amounts of the binary halides NaI, SmI_2, and TlI by the vertical Bridgman technique. NaI (>99.5%, Merck KGaA) and TlI (99.999%, Alfa) were dried at 200 °C in vacuum. SmI_2 was synthesised from SmI_3 and Sm (>99.9%, Alfa) in a Ta ampoule, which was sealed by He arc welding and encapsulated in a silica ampoule under vacuum. SmI_3 was prepared from Sm and I_2 (p.a., Merck KGaA) in a sealed silica ampoule and sublimated for purification in a silica apparatus under high vacuum. All crystals were grown in Ta ampoules with a typical batch size of 2.5 g. A small excess of Sm (10 mg per batch) ensured that all crystals contain divalent Sm^{2+}, only. The Ta ampoules were heated to 680 °C for one day, i.e. above the melting point of NaI at 662 °C, slowly cooled by 1 K/h to 550 °C, and then by 5 K/h to room temperature. The Sm^{2+} and Tl^+ concentrations refer to the nominal concentration in the melt. Crystal pieces were selected from the product, some were sealed in small silica ampoules under He gas for spectroscopic investigations. Fig. 1 shows the intense green colour of millimeter sized NaI:0.2%Sm^{2+} and NaI:0.2%Tl^+,0.2%Sm^{2+} crystals. All handling of starting materials and products was done under strictly dry conditions in glove boxes (H_2O and O_2 <0.1 ppm) or sealed sample containers. The materials are very hygroscopic and Sm^{2+} oxidises rapidly, e.g. in contact with air, which becomes obvious by the disappearance of the dark green colour of the crystals.

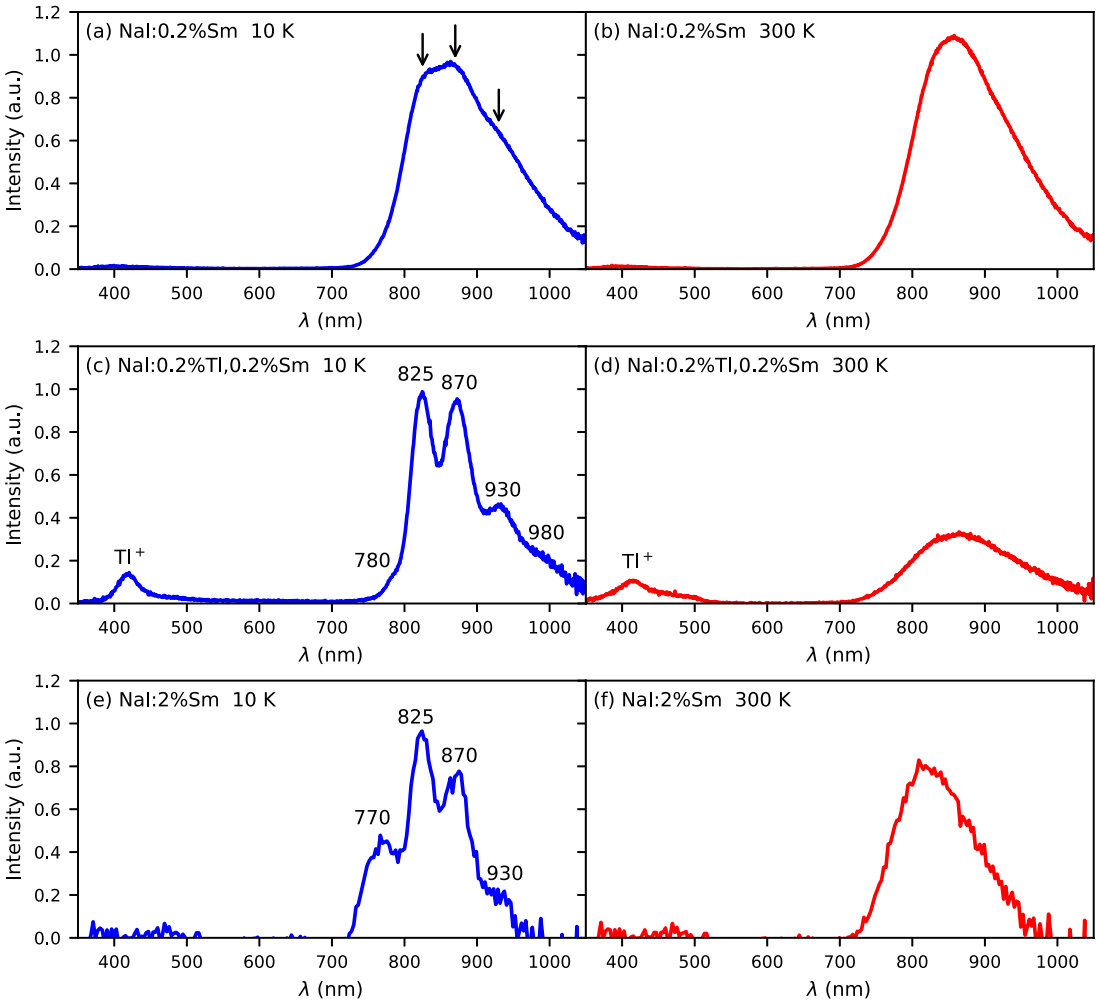

Fig. 3. X-ray excited emission spectra of NaI:0.2%Sm^{2+} at (a) 10 K and (b) 300 K; NaI:0.2%Tl^{+},0.2%Sm^{2+} at (c) 10 K and (d) 300 K; NaI:2%Sm^{2+} at (e) 10 K and (f) 300 K.

X-ray excited emission spectra were recorded using a Varex VF-80JM X-ray tube with tungsten anode operated at 80 kV and 1 mA to excite the sample. The low energy X-rays were removed using a 1 mm thick copper filter to prevent potential radiation damage to the sample. The sample holder was mounted on the cold finger of a Janis He or N_2 cryostat. The sample chamber was kept at a pressure below 10^{-4} mbar during measurement. The emission light coming from the sample under a 90° angle with respect to the X-ray beam was coupled into an optical fibre and detected using an Ocean Insight QEPro spectrometer. The temperature of the sample was controlled using a Lakeshore temperature controller.

Photoluminescence emission spectra were measured using a 450 W xenon lamp and Horiba Gemini 180 monochromator as excitation source. The rest of the set-up was identical to the set-up used for measurements under X-ray excitation, with the exception that here an optical filter was placed between sample and optical fibre to filter out the excitation light. For photoluminescence excitation spectra, the emission light from the sample passed through a SpectraPro-SP2358 monochromator before being detected using a Hamamatsu R7600U-20 PMT. Corrections for the xenon lamp spectrum and transmission of the excitation monochromator were performed by measuring the intensity of the excitation light using an Opto Diode UVG100 photodiode.

Photoluminescence decay curves were measured using an EKSPLA NT230 OPO laser as excitation source. The laser has a pulse duration of 6 ns and was used with a repetition rate of 100 Hz. The sample chamber and detection equipment were the same as used for the photoluminescence excitation spectra. The signal coming from the Hamamatsu R7600U-20 PMT was recorded using a CAEN DT5730 digitiser. The signals of multiple pulses were added up using the trigger signal coming from laser driver.

Pulse height spectra were recorded using a Broadcom AFBR-S4N44P014M SiPM as photodetector with 32.5 V breakdown voltage. A reverse bias voltage of 45 V was used. The scintillator was placed on top of the 4 × 4 mm^2 sensitive area of the detector and surrounded by a PTFE dome to reflect all the scintillation light towards the SiPM. The signal was integrated using a 56 nF capacitor placed in parallel with a 1.8 kΩ resistor to create an electronic signal with longer than 50 μs decay time required for the input of the Ortec 672 spectroscopic amplifier. The spectroscopic amplifier was used with a shaping time of 10 μs. Its output signal was read out using an Ortec 926 multichannel analyser.

3. Results

The X-ray excited emission spectrum of NaI:0.2%Sm^{2+} at 10 K is shown in Fig. 3a. It shows a broad emission band starting at 750 nm that still has significant intensity at 1050 nm. This band is ascribed to the Sm^{2+} $4f^55d \rightarrow 4f^6$ emission, as the wavelength corresponds well with expectation based on the emission wavelength of the Eu^{2+} in NaI [38]. The full width at half maximum of the emission band is 0.27 eV, which is much broader than the typical 0.15 eV for Sm^{2+} $4f^55d \rightarrow 4f^6$ emission at cryogenic temperatures [44,45]. The band contains structure around 825, 870 and 930 nm, which has been marked with

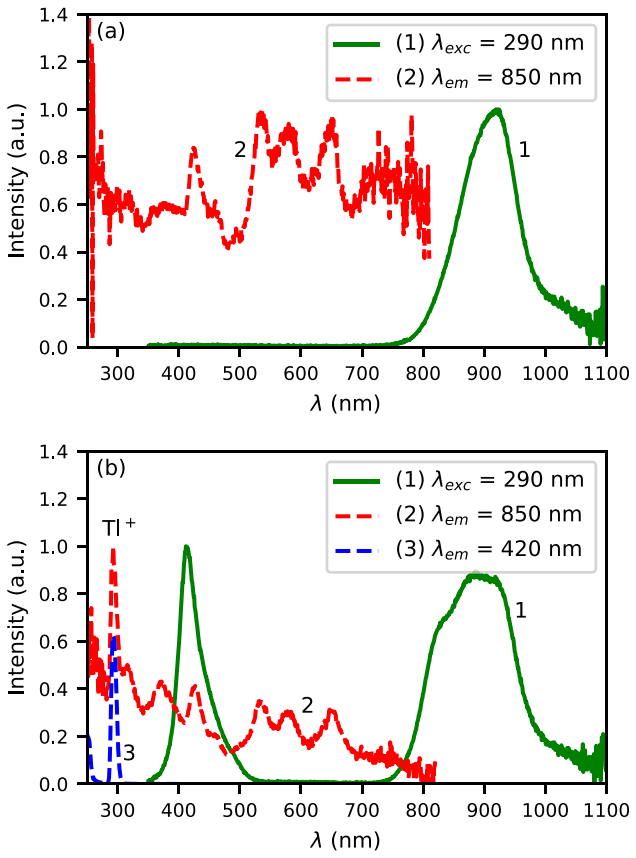

Fig. 4. Photoluminescence excitation and emission spectra of (a) NaI:0.2%Sm^{2+} and (b) NaI:0.2%Tl^{+},0.2%Sm^{2+}. The Tl^{+} A-band at 290 nm in (b) is visible in the excitation spectrum of Sm^{2+}, indicating energy transfer from Tl^{+} to Sm^{2+}.

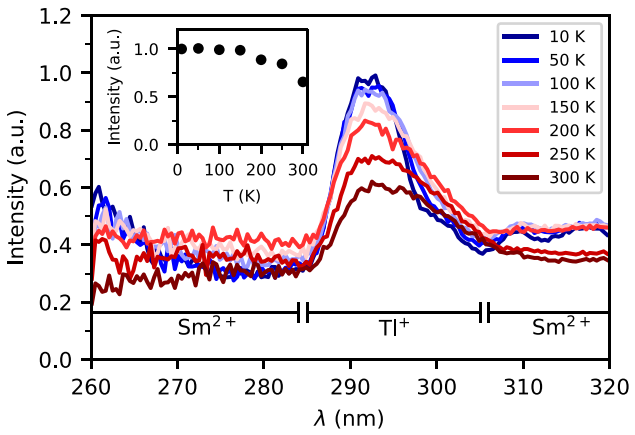

Fig. 5. Photoluminescence excitation spectra of the Sm^{2+} emission in NaI:0.2%Tl^{+},0.2%Sm^{2+} between 260 nm and 320 nm. The Sm^{2+} emission is monitored at 850 nm. With increasing temperature, the intensity of the Tl^{+} A-band decreases while the intensity of the Sm^{2+} $4f^6 \rightarrow 4f^5 5d$ excitation bands stays the same.

arrows. Fig. 3b shows that the emission band does not become significantly broader with temperature, but the structure within the band becomes less pronounced. This suggests that Sm^{2+} emission originates from multiple sites, each with their own emission wavelength. Broadening of each emission band with temperature removes the structure in the emission band, but as the emission wavelength of each band does not change much, the total width of the emission band remains mostly unaffected. The total intensity of the emission remains constant within measurement error.

Fig. 3c shows the X-ray excited emission spectrum of NaI:0.2%Tl^{+}, 0.2%Sm^{2+} at 10 K. Compared to the spectrum of NaI:0.2%Sm^{2+} in Fig. 3a, the different emission bands are more resolved. The labels in the figure correspond to the wavelength at which each of the emission bands is at highest intensity. The bands at 780, 825, and 870 nm were also observed by Guzzi and Baldini [22]. The bands at 930 and 980 nm were not found due to the low sensitivity of their detector in that wavelength range, but it is likely that these bands were also present in the emission spectrum of their sample. In addition to the Sm^{2+} $4f^5 5d \rightarrow 4f^6$ emission, also a weak emission band around 420 nm is observed. This emission band is ascribed to Tl^{+} [46].

Fig. 3d shows the X-ray excited emission spectrum of NaI:0.2%Tl^{+}, 0.2%Sm^{2+} at 300 K. Compared to the emission spectrum at 10 K (Fig. 3c), the Sm^{2+} emission intensity has decreased by about 50%. This is different from the NaI:0.2%Sm^{2+} sample (Fig. 3a and b), where the Sm^{2+} emission intensity remained constant.

The 10 K X-ray excited emission spectrum of NaI:2%Sm^{2+} in Fig. 3e also shows multiple resolved emission bands. 3 emission bands, namely the ones at 825, 870, and 930 nm, are positioned at the same wavelength as the emission bands in NaI:0.2%Tl^{+},0.2%Sm^{2+} (Fig. 3c). The emission band at 770 lies at slightly shorter wavelength than the 780 nm emission band in NaI:0.2%Tl^{+},0.2%Sm^{2+}. No emission band was observed near 980 nm. When increasing the temperature to 300 K (Fig. 3f), the Sm^{2+} emission does not show a decrease in intensity. This suggests that the decrease in Sm^{2+} emission intensity in NaI:0.2%Tl^{+},0.2%Sm^{2+} (Fig. 3d compared to c) is caused by co-doping with Tl^{+}.

To further investigate the role of energy transfer from Tl^{+} to Sm^{2+}, Fig. 4 compares the photoluminescence excitation and emission spectra of NaI:0.2%Sm^{2+} and NaI:0.2%Tl^{+},0.2%Sm^{2+} at 10 K. The spectra of NaI:0.2%Sm^{2+} are shown in Fig. 4a. The emission spectrum under excitation with 290 nm light (Curve 1) again shows exclusively Sm^{2+} $4f^5 5d \rightarrow 4f^6$ emission. The excitation spectrum monitoring the Sm^{2+} emission at 850 nm (Curve 2) contains many broad bands spanning across the entire visible spectrum.

The emission spectrum of NaI:0.2%Tl^{+},0.2%Sm^{2+} excited with 290 nm light (Fig. 4b Curve 1) shows both Tl^{+} emission around 420 nm and Sm^{2+} emission around 900 nm. The Tl^{+} emission is visible because 290 nm lights corresponds to the wavelength of the Tl^{+} A-band [47]. This absorption band is visible in the excitation spectrum when monitoring the Tl^{+} emission at 420 nm (Curve 3), but also when monitoring the Sm^{2+} emission at 850 nm (Curve 2). This means that excitation of Tl^{+} results in Sm^{2+} emission, and therefore it can be concluded that Tl^{+} transfers energy to Sm^{2+}.

Even though Tl^{+} transfers energy to Sm^{2+}, the intensity of the Tl^{+} emission is almost equal to that of the Sm^{2+} emission in Fig. 4b. The ratio between the Tl^{+} and Sm^{2+} emission is also much higher than in the emission spectrum under X-ray excitation (Fig. 3c). This is likely caused by the penetration depth of the photons exciting the sample. 290 nm light is strongly absorbed by both Tl^{+} and Sm^{2+}, meaning all excitations occur near the sample surface, which is the same side that is facing the detector. The X-rays used to excite the sample have a much larger penetration depth and excite the bulk of the sample uniformly. Therefore the Tl^{+} emission needs to travel a longer distance through the crystals compared to optical excitation. The lower intensity of the Tl^{+} emission under X-ray excitation can therefore be interpreted as an increase in radiative energy transfer, meaning the efficiency of nonradiative energy transfer is low. This is also expected due to the relatively low Sm^{2+} concentration of 0.2%.

The decrease in intensity of the Sm^{2+} emission intensity in NaI: 0.2%Tl^{+},0.2%Sm^{2+} at 300 K compared to 10 K (Fig. 3c and d) seems to have something to do with Tl^{+} co-doping. To get more information about the stage of the scintillation process in which excitation are lost, part of the excitation spectrum of the Sm^{2+} emission monitored at

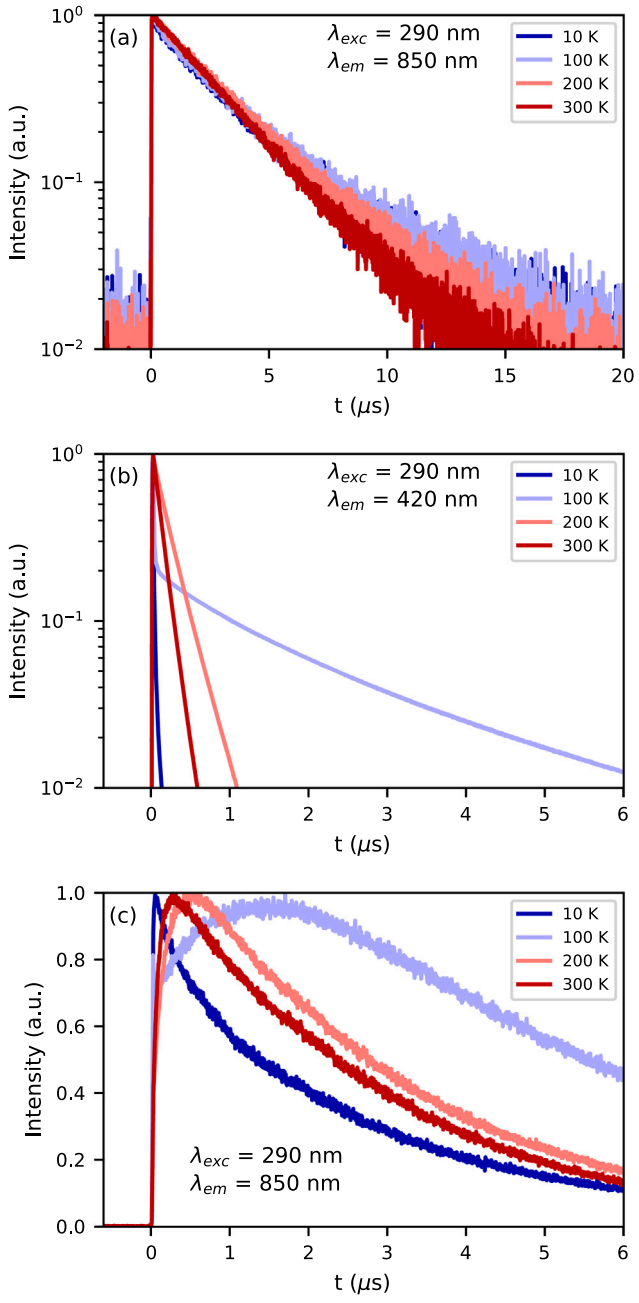

Fig. 6. Photoluminescence decay curves excited at 290 nm of (a) Sm^{2+} emission in NaI:0.2%$^{2+}$ at 850 nm, (b) Tl^{+} emission in NaI:0.2%Tl^{+},0.2%$^{2+}$ at 420 nm, and (c) Sm^{2+} emission in NaI:0.2%Tl^{+},0.2%$^{2+}$ at 850 nm. Note the linear intensity scale in (c).

850 nm at temperatures between 10 K and 300 K is shown in Fig. 5. The wavelength range that is shown contains the Tl^{+} A-band excitation around 290 nm. The inset shows the total integrated intensity of this Tl^{+} band. This was calculated by interpolating the Sm^{2+} $4f^6 \rightarrow 4f^5 5d$ excitation bands and subtracting it from the wavelength range between 285 nm and 305 nm. The integrated intensity of the Tl^{+} A-band starts to decrease above 200 K. At the same time, the intensity of the Sm^{2+} $4f^6 \rightarrow 4f^5 5d$ excitation bands does not decrease. This shows that the Sm^{2+} emission is not quenched due to the presence of Tl^{+}. Instead, the excitations are lost already before energy transfer from Tl^{+} to Sm^{2+} occurs.

Fig. 6 shows the photoluminescence decay of the NaI:0.2%Sm^{2+} and NaI:0.2%Tl^{+},0.2%Sm^{2+} under 290 nm excitation. The decay time constants are summarised in Table 1. Fig. 6a shows the photoluminescence decay of the Sm^{2+} emission in NaI:0.2%Sm^{2+} between 10 K and 300 K. The sample was excited with 290 nm light and the emission was monitored at 850 nm. The emission shows approximately single exponential decay at all temperatures. The decay time is 2.8 μs, in accordance with the <3 μs reported by Guzzi and Baldini [22]. No components with rise time are observed.

Table 1
Overview of the photoluminescence decay and rise time constants in NaI:0.2%Sm^{2+} and NaI:0.2%Tl^{+},0.2%Sm^{2+} as a function of temperature. Subscripts "d" and "r" denote the decay and rise time constants, respectively. Subscripts "Sm" and "Tl" denote the ion of which the emission is monitored. Two components were observed at 50 K, the percentages reflect their relative intensities.

T (K)	NaI:0.2%Sm^{2+}	NaI:0.2%Tl^{+},0.2%Sm^{2+}		
	$\tau_{d,Sm}$ (μs)	$\tau_{d,Tl}$ (μs)	$\tau_{r,Sm}$ (μs)	$\tau_{d,Sm}$ (μs)
10	2.8	0.09	–	2.8
50	2.8	0.01 (5%) 35 (95%)	–	2.8 (25%) 35 (75%)
100	2.8	3.2	1.3	3.2
150	2.8	0.65	0.45	3.0
200	2.8	0.32	0.32	2.8
250	2.8	0.15	0.11	2.9
300	2.8	0.12	0.10	2.8

When exciting NaI:0.2%Tl^{+},0.2%Sm^{2+} at 290 nm, Tl^{+} emission was observed in addition to the Sm^{2+} emission (Fig. 4b). The photoluminescence decay of the Tl^{+} emission monitored at 420 nm is shown in Fig. 6b. It shows complicated temperature behaviour, where at 10 K only a fast component with decay time of around 10 ns is visible above the noise. Increasing the temperature to 100 K decreases the intensity of this fast component and a slow component with decay time of 3.2 μs becomes dominant. Further increase of the temperature to 200 K and 300 K makes the fast component disappear and shortens the decay time of the slow component. At 300 K, the decay time is 125 ns. This complex temperature behaviour is characteristic of Tl^{+} emission in NaI:Tl^{+} [48,49]. The intrinsic decay time at 300 K of Tl^{+} emission in NaI is 250 ns [50]. The 125 ns decay time of the Tl^{+} emission in NaI:0.2%Tl^{+},0.2%Sm^{2+} shows that approximately 50% of the excitations are transferred from Tl^{+} to Sm^{2+} nonradiatively.

As Tl^{+} transfers its excitations to Sm^{2+}, this also affects the luminescence decay of Sm^{2+}. Monitoring the Sm^{2+} emission at 850 nm, again complex temperature behaviour is observed. All decay traces have a component with rise time. At 10 K, this rise time is the shortest with a value of about 10 ns, corresponding to the fast decay of Tl^{+} at this temperature. At 100 K, the remaining fast component of the Tl^{+} emission combined with some Sm^{2+} being excited directly by the laser causes what is perceived as an initial step, followed by a slow rise time component caused by the slow decay component of Tl^{+}. This slow rise time then becomes progressively shorter as the temperature is increased to 200 K and 300 K.

It is reported in literature that NaI:Eu^{2+} crystals are typically opaque when grown from a melt. They can be made transparent by annealing the sample and subsequently quenching it back to room temperature. In this process, the precipitates containing Eu^{2+} dissolve into the NaI host, reducing the associated scattering of light. The annealing temperature is typically around 400 °C [16,17,21]. As Sm^{2+} is chemically very similar to Eu^{2+}, it is likely that the samples studied in this work are also opaque. It is however difficult to see by eye, as the strong Sm^{2+} absorption bands make the crystals appear black. Therefore, the effect of heat treatment is studied by monitoring the photoluminescence intensity while increasing the temperature of the sample. The wait time was 20 min between measurements to allow the temperature to stabilise. The photoluminescence spectra are shown in Fig. 7a-c. Fig. 7d shows the integrated photoluminescence intensity over the entire temperature range.

Fig. 7a shows the photoluminescence emission spectra when heating from 300 K to 450 K. In this temperature range the emission bands

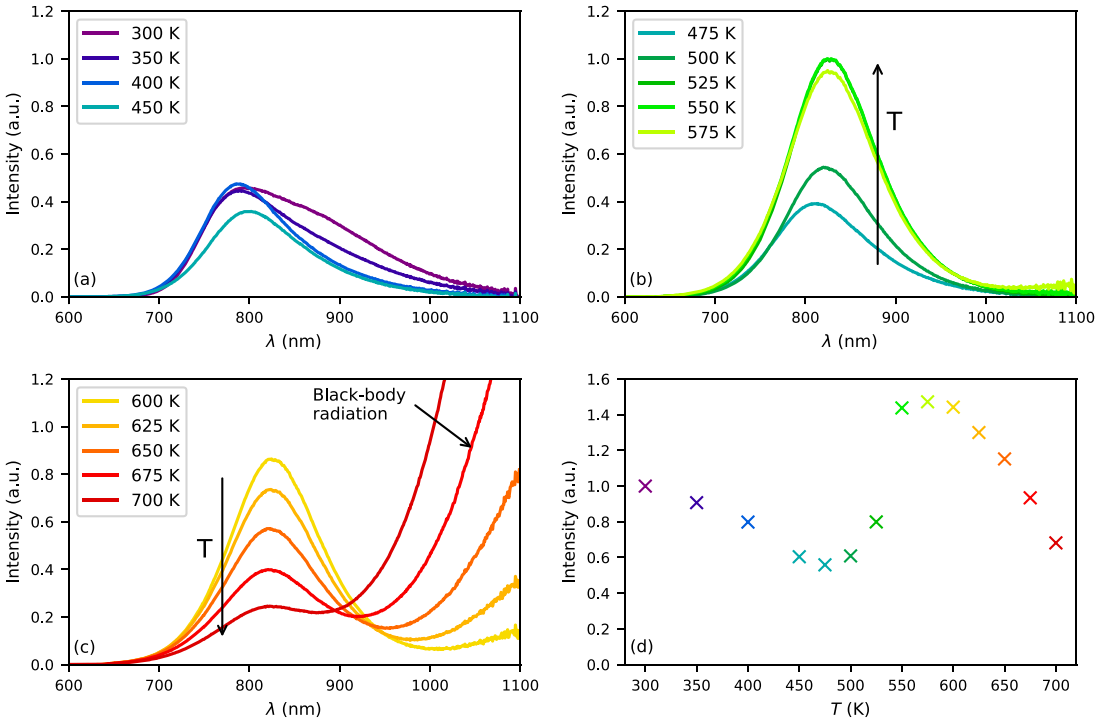

Fig. 7. The change in photoluminescence emission spectra of NaI:2%Sm^{2+} excited at 500 nm under increasing temperature. (a) between 300 K and 450 K only minor changes in spectral shape are observed, (b) between 475 K and 575 K the intensity increases by a factor 2.5, (c) above 600 K thermal quenching causes the emission intensity to decrease, (d) the integrated photoluminescence intensity as a function of temperature.

around 900 nm start to disappear, while the emission bands around 800 nm retain their intensity. The result is a decrease in total luminescence intensity by about 40%. Fig. 7b shows the temperature range between 475 K and 575 K. Between 475 K and 525 K, an increase of the luminescence intensity by almost a factor 2.5 is observed. The temperature at which this happens is below typical annealing temperatures which are used in literature for making initially opaque NaI:Eu^{2+} or NaI:Sm^{2+} crystals transparent [16,17,21,22]. Further increase in temperature to 575 K has almost no effect on the luminescence intensity until around 600 K (Fig. 7c) thermal quenching of the Sm^{2+} emission causes the emission intensity to decrease again.

As heating the samples increases the intensity of the photoluminescence signal, it was tested whether annealing the samples would have a positive effect on the scintillation properties of NaI:Sm^{2+}. Fig. 8a shows the ^{137}Cs excited pulse height spectrum of an as grown NaI:0.2%Sm^{2+} crystal of about 1 mm^3 size. It also shows the pulse height spectrum for the same sample after annealing at 550 K for 30 min and subsequent quenching by placing the crystal on a block of stainless steel at room temperature. Annealing the sample moves the photopeak to 2.2 times higher channel and improves the energy resolution from 15% to 11%. The same is done for NaI:0.2%Tl^+,0.2%Sm^{2+} in Fig. 8b. A similar shift in the photopeak to higher channel is observed and the energy resolution improves from 22% to 11%. Using this set up, only a rough estimate of the light yield could be made using NaI:Tl^+ as reference sample. The light yield of the annealed samples was estimated between 20,000 ph/MeV and 50,000 ph/MeV, similar to NaI:Eu^{2+} reports in literature [13].

Since NaI:Eu^{2+} is reported to have changing emission properties over time and divalent doping is known to increase the ionic conductivity in alkali halides, it is not obvious that these improved scintillation properties are permanent. To see how long the improvements to the light yield and energy resolution last, the NaI:0.2%Sm^{2+} sample was annealed and quenched again. Directly after this, a series of pulse height spectra was recorded, with a recording time of each spectrum being 30 min. The results are shown in Fig. 9. Directly after annealing,

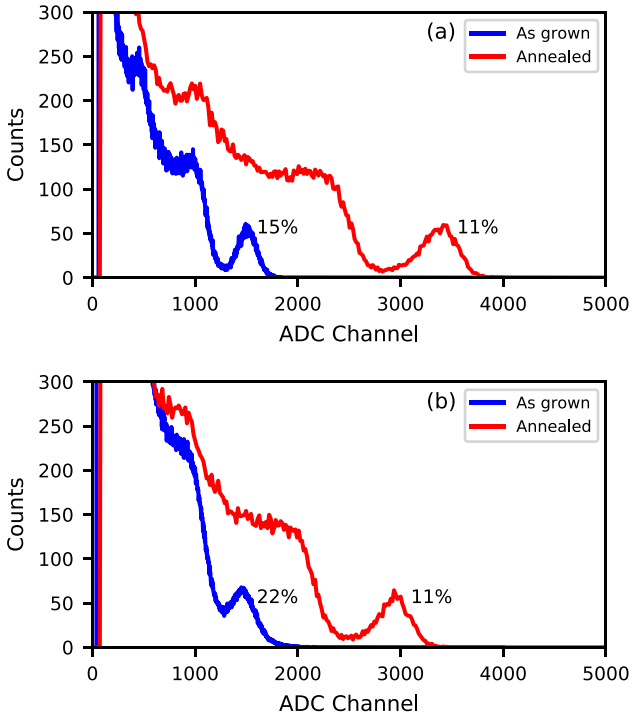

Fig. 8. ^{137}Cs excited pulse height spectra before and after annealing and quenching of (a) NaI:0.2%Sm^{2+} and (b) NaI:0.2%Tl^+,0.2%Sm^{2+}.

the photopeak is again at the same channel as it was after annealing in Fig. 8a. However, after 1 day, the photopeak has already shifted to almost 20% lower channel, indicating that the changes caused by annealing do not result in a long lasting improvement of the scintillation properties at room temperature. The change is so fast that recording a

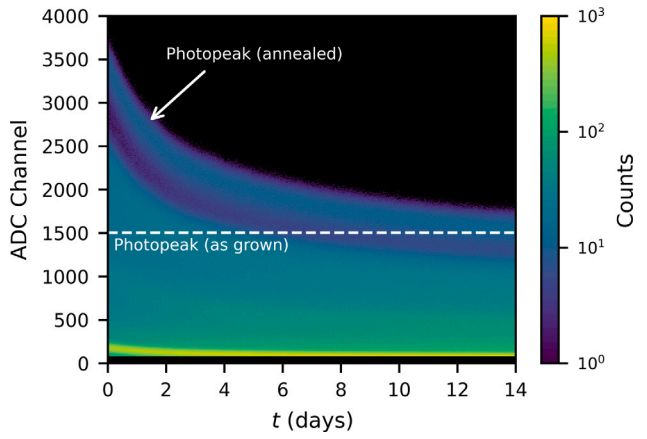

Fig. 9. ^{137}Cs excited pulse height spectra of NaI:0.2%Sm^{2+} on a SiPM plotted against time after annealing and subsequent quenching. The photopeak moves back to where its position was before annealing, significant changes are already visible within hours.

pulse height spectrum for several hours directly after annealing would result in the photopeak being smeared out, significantly worsening the energy resolution. After approximately 14 days, the position of the photopeak is back to where it was before annealing.

4. Discussion

The Sm^{2+} $4f^55d \rightarrow 4f^6[^7F_0]$ transition always lies at around 1.22 eV lower energy than the $4f^65d \rightarrow 4f^7$ emission of Eu^{2+} when occupying the same site [38]. However, the ratio between the different $4f^55d \rightarrow 4f^6[^7F_J]$ may vary between sites, making it difficult to directly compare the Eu^{2+} emission wavelength to that of Sm^{2+}. Attempting to pair each Sm^{2+} to an Eu^{2+} emission band by translating all Sm^{2+} emission maxima to around 1.22 eV higher energy was therefore not successful. However, the fact that 5 different Sm^{2+} sites could be identified still suggests that the charge compensation mechanism and site formation is the same for NaI:Sm^{2+} and NaI:Eu^{2+}. This is also in line with expectation, as Sm^{2+} and Eu^{2+} have the same charge and very similar ionic radius.

To efficiently read out the Sm^{2+} emission with silicon based photodetectors, the majority of the X-ray excited emission spectrum needs to lie at wavelengths shorter than 800 nm. Fig. 3 shows that this is not the case for any of the samples. Out of the 5 different Sm^{2+} sites that have been identified, only the site which has an emission maximum at 770 nm emits at shorter wavelength than 800 nm. Ideally, all emission would originate from this site. The emission spectrum of NaI:Eu^{2+} depends strongly on things like synthesis method, sample age, and excitation method. The 770 nm Sm^{2+} emission is the shortest wavelength Sm^{2+} emission band and therefore likely originates from the same type of site as the 410 nm emission band of Eu^{2+} found by Shiran et al. (Fig. 2a [17]).

Shiran et al. showed that the relative intensity of the 410 nm and 439 nm emission bands increase when the Eu^{2+} concentration is 0.1% or lower [17]. It is likely that Sm^{2+} shows the same behaviour and using a lower concentration may increase the intensity of the 770 nm band under X-ray excitation. Opposite to this trend, however, the data in Fig. 3 show that increasing the Sm^{2+} concentration actually increases the relative intensity of the 770 nm emission band. Shiran et al. did not research samples with a concentration as high as 2%, and potentially this is would also be observed for Eu^{2+} emission in samples with such high doping concentration.

When co-doping Tl^+ and Eu^{2+} in NaI, the Tl^+ emission is almost entirely replaced by Eu^{2+}, even at Eu^{2+} below 0.1% [13,19]. In the case of co-doping NaI:Tl^+ and Sm^{2+}, it was shown that energy transfer also takes place from Tl^+ to Sm^{2+}. However, even at a Sm^{2+} concentration of 0.2%, the energy was transferred for a large part radiatively. Drastically lowering the Sm^{2+} concentration in an attempt to increase the intensity of the 770 nm emission band would therefore make the energy transfer inefficient. Additionally, since Tl^+ seems to decrease the intensity of the Sm^{2+} emission at room temperature, co-doping these two ions does not seem to yield desired scintillation characteristics. It is therefore better to use Sm^{2+} as the only dopant.

It was demonstrated in Fig. 7 that the emission intensity of NaI:Sm^{2+} increases significantly upon reaching a temperature of around 525 K. This temperature roughly coincides with typical annealing temperatures found in literature that is used to make opaque NaI:Eu^{2+} scintillator crystals transparent [16,17,21,22]. It was also demonstrated in Fig. 8 that heating to 550 K and subsequently quenching the NaI:Sm^{2+} crystals significantly improves both the light yield and energy resolution. It is therefore likely that during the annealing process, precipitates containing Sm^{2+} dissolve and Sm^{2+} redistributes through the host lattice. This is also in line with the emission bands at 870 nm and longer wavelength disappearing from the emission spectrum in Fig. 7a upon heating the sample (Fig. 7a), which is then interpreted as the disappearing of the emission bands originating from the precipitates. A homogeneous distribution of Sm^{2+} through the host lattice would thus result in a higher light yield.

Unfortunately, the positive effects of annealing rapidly disappear and the samples return to their original properties in approximately 14 days (Fig. 9). The high ionic conductivity of Sm^{2+} in NaI allows formation of new precipitates. The rate at which the degradation of the light yield occurs is so fast that even a pulse height spectrum measured over the course of several hours will be significantly distorted. Because of this, it is difficult to imagine that the positive effects of annealing NaI:Sm^{2+} will have any practical application, unless a method can be found to stabilise the samples after annealing them. For this, it is likely that the ionic conductivity of the crystals needs to be suppressed. It has been shown experimentally that this can be achieved in NaCl by doping with divalent anions, such as S^{2-} [51], which could serve as charge compensation for Eu^{2+} or Sm^{2+} and prevent the creation of cation vacancies. Co-doping NaI:Eu^{2+} and NaI:Sm^{2+} with O^{2-} or S^{2-} may therefore be a logical next step to improve their scintillation properties.

5. Conclusions

Sm^{2+} was investigated as an activator for NaI scintillators. While the NaI lattice has only one cation site, Sm^{2+} emission was observed from at least 5 different sites. The nature of these sites remains unknown, but strong similarities were found between the site formation of Sm^{2+} and Eu^{2+} reported in literature. The emission wavelength of 4 out of 5 sites is longer than 800 nm, which is too long for efficient read out with silicon based photodetectors. Furthermore, it was found that co-doping Tl^+ and Sm^{2+} reduces Sm^{2+} emission intensity under X-ray excitation. Similar to NaI:Eu^{2+}, the scintillation properties of NaI:Sm^{2+} significantly improve upon annealing and subsequent quenching. The energy resolution attained with a silicon photomultiplier improved from 15% to 11% for NaI:0.2%Sm^{2+} and from 22% to 11% for NaI:0.2%Tl^+,0.2%Sm^{2+}. However, these improved properties completely disappeared again over the course of two weeks.

CRediT authorship contribution statement

Casper van Aarle: Writing – original draft, Visualization, Investigation, Conceptualization. **Daniel A. Biner:** Resources. **Karl W. Krämer:** Writing – review & editing, Resources. **Pieter Dorenbos:** Writing – review & editing, Funding acquisition.

Declaration of competing interest

The authors declare that they have no known competing financial interests or personal relationships that could have appeared to influence the work reported in this paper.

Data availability

Data will be made available on request.

Acknowledgements

This research was subsidised by the TTW/OTP grant no. 18040 of the Dutch Research Council. The authors would like to thank Stefan Brunner from Broadcom Inc. for making the SiPMs available.

References

[1] Robert Hofstadter, Phys. Rev. 74 (1948) 100.
[2] Robert Hofstadter, Phys. Rev. 75 (1949) 796.
[3] R. Hofstadter, J.A. McIntyre, Phys. Rev. 80 (1950) 631.
[4] Giulia Hull, Woon-Seng Choong, William W. Moses, Gregory Bizarri, John. D. Valentine, Stephen A. Payne, Nerine J. Cherepy, Bryan W. Reutter, IEEE Trans. Nucl. Sci. 56 (2009) 331.
[5] P. Dorenbos, J.T.M. de Haas, C.W.E. van Eijk, IEEE Trans. Nucl. Sci. 42 (1995) 2190.
[6] M. Moszyński, W. Czarnacki, M. Kapusta, M. Szawlowski, W. Klamra, P. Schotanus, Nucl. Instrum. Methods A 486 (2002) 13.
[7] M. Moszyński, J. Zalipska, M. Balcerzyk, M. Kapusta, W. Mengesha, J.D. Valentine, Nucl. Instrum. Methods A 484 (2002) 259.
[8] M. Moszyński, M. Balcerzyk, W. Czarnacki, M. Kapusta, W. Klamra, P. Schotanus, A. Syntfeld, M. Szawlowski, IEEE Trans. Nucl. Sci. 50 (2003) 767.
[9] M. Moszyński, W. Czarnacki, W. Klamra, M. Szawlowski, P. Schotanus, M. Kapusta, Nucl. Instrum. Methods A 505 (2003) 63.
[10] M.S. Alekhin, J.T.M. de Haas, I.V. Khodyuk, K.W. Krämer, P.R. Menge, V. Ouspenski, P. Dorenbos, Appl. Phys. Lett. 102 (2013) 151915.
[11] E.V.D. van Loef, P. Dorenbos, C.W.E. van Eijk, K. Krämer, H.U. Güdel, Appl. Phys. Lett. 79 (2001) 1573.
[12] K. Yang, P.R. Menge, J. Appl. Phys. 118 (2015) 213106.
[13] I.V. Khodyuk, S.A. Messina, T.J. Hayden, E.D. Bourret, G.A. Bizarri, J. Appl. Phys. 118 (2015) 084901.
[14] Jingkang Wang, Chenger Wang, Huanyin Li, Jian Shi, Xuemin Wen, Chenyu Shan, Guohao Ren, Xilei Sun, Yuntao Wu, IEEE Trans. Nucl. Sci. 70 (2023) 840.
[15] J.A. Hernandez, F.J. Lopez, H.S. Murrieta, J.O. Rubio, J. Phys. Soc. Japan 50 (1981) 225.
[16] F.J. López, H.S. Murrieta, J.A. Hernández, J.O. Rubio, J. Lumin. 26 (1981) 129.
[17] N. Shiran, A. Gektin, Y. Boyarintseva, S. Vasyukov, A. Boyarintsev, V. Pedash, S. Tkachenko, O. Zelenskaya, D. Zosim, Opt. Mater. 32 (2010) 1345.
[18] Natalia V. Shiran, Alexander V. Gektin, Yanina Boyarintseva, Sergey Vasyukov, Andrej Boyarintsev, Vyacheslav Pedash, Sergej Tkachenko, Olga Zelenskaya, N. Kosinov, O. Kisil, L. Philippovich, IEEE Trans. Nucl. Sci. 57 (2010) 1233.
[19] S. Gridin, S. Vasyukov, N. Shiran, A. Gektin, Funct. Mater. 21 (2014) 498.
[20] N. Shiran, A. Gektin, Ia. Boiaryntseva, S. Vasyukov, S. Gridin, A. Belsky, J. Lumin. 164 (2015) 64.
[21] Manuel Ulreich, Lynn A. Boatner, Igor Sokolović, Michele Reticcioli, Berthold Stoeger, Flora Poelzleitner, Cesare Franchini, Michael Schmid, Ulrike Diebold, Martin Setvin, Phys. Rev. Mater. 3 (2019) 075004.
[22] M. Guzzi, G. Baldini, J. Lumin. 6 (1973) 270.
[23] P. Dorenbos, J. Lumin. 104 (2003) 239.
[24] N. Brown, I.M. Hoodless, J. Phys. Chem. Solids 28 (1967) 2297.
[25] R.W. Dreyfus, A.S. Nowick, Phys. Rev. 126 (1962) 1367.
[26] A.B. Lidiard, Ionic conductivity, in: Electrical Conductivity II, in: Encyclopedia of Physics, vol. 4 / 20, Springer, 1957.
[27] Tuchen Huang, Qibin Fu, Shaopeng Lin, Biao Wang, Nucl. Instrum. Methods Phys. Res. A 851 (2017) 118.
[28] Junhyeok Kim, Kyeongjin Park, Jisung Hwang, Hojik Kim, Jinhwan Kim, Hyunduk Kim, Sung-Hee Jung, Youngsug Kim, Gyuseong Cho, Nucl. Eng. Technol. 51 (2019) 1091.
[29] Maheng Ye, Pin Gong, Sunci Wu, Yong Li, Cheng Zhou, Xiaoxiang Zhu, Xiaobin Tang, Appl. Radiat. Isot. 176 (2021) 109848.
[30] Fengzhao Shen, Qibin Fu, Tuchen Huang, Wei Wang, Crystals 12 (2022) 1077.
[31] Claudio Piemonte, Alberto Gola, Nucl. Instrum. Methods Phys. Res. A 926 (2019) 2.
[32] D. Guberman, R. Paoletti, A. Rugliancich, C. Wunderlich, A. Passeri, Phys. Medica 82 (2021) 171.
[33] S. Vinogradov, E. Popova, Nucl. Instrum. Methods Phys. Res. A 952 (2020) 161752.
[34] G.H. Dieke, R. Sarup, J. Chem. Phys. 36 (1962) 371.
[35] Julien Christmann, Hans Hagemann, J. Phys. Chem. A 123 (2019) 2881.
[36] Markus Suta, Claudia Wickleder, J. Lumin. 210 (2019) 210.
[37] Jafar Afshani, Teresa Delgado, Gheorghe Paveliuc, Prodipta Pal, Hans Hagemann, J. Lumin. 257 (2023) 119648.
[38] P. Dorenbos, J. Phys. Condens. Matter 15 (2003) 575.
[39] Casper van Aarle, Karl W. Krämer, Pieter Dorenbos, J. Lumin. 266 (2024) 120329.
[40] R.H.P. Awater, M.S. Alekhin, D.A. Biner, K.W. Krämer, P. Dorenbos, J. Lumin. 212 (2019) 1.
[41] Weronika Wolszczak, Karl W. Krämer, Pieter Dorenbos, Phys. Status Solidi R. 13 (2019) 1900158.
[42] Casper van Aarle, Karl W. Krämer, Pieter Dorenbos, J. Lumin. 238 (2021) 118257.
[43] Casper van Aarle, Nils Roturier, Daniel A. Biner, Karl W. Krämer, Pieter Dorenbos, Opt. Mater. 145 (2023) 114375.
[44] Mikhail S. Alekhin, Roy H.P. Awater, Daniel A. Biner, Karl W. Krämer, Johan T.M. de Haas, Pieter Dorenbos, J. Lumin. 167 (2015) 347.
[45] Casper van Aarle, Karl W. Krämer, Pieter Dorenbos, J. Lumin. 251 (2022) 119209.
[46] D.W. Aitken, B.L. Beron, G. Yenicay, H.R. Zulliger, IEEE Trans. Nucl. Sci. 14 (1967) 468.
[47] A. Ranfagni, D. Mugnai, M. Bacci, G. Viliani, M.P. Fontana, Adv. Phys. 32 (1983) 823.
[48] S. Benci, M.P. Fontana, M. Manfredi, Phys. Status Solidi b 81 (1977) 603.
[49] V. Yakovlev, L. Trefilova, V. Alekseev, V. Krasnov, Funct. Mater. 23 (2016) 540.
[50] J.S. Schweitzer, W. Ziehl, IEEE Trans. Nucl. Sci. 30 (1983) 380.
[51] Mamoru Baba, Tashio Ikeda, Shigetomo Yoshida, Japan. J. Appl. Phys. 14 (1975) 1273.